The current issue and full text archive of this journal is available at
www.emeraldinsight.com/0961-5539.htm

Lattice Boltzmann method simulation gas slip flow in long microtubes

Haibo Huang, T.S. Lee and C. Shu
Fluid Division, Department of Mechanical Engineering, National University of Singapore, Singapore

Received 8 November 2005
Revised 20 February 2006
Accepted 8 March 2006

Abstract

Purpose – This paper aims to examine how using lattice Boltzmann method (LBM) aids the study of the isothermal-gas flow with slight rarefaction in long microtubes.

Design/methodology/approach – A revised axisymmetric lattice Boltzmann model is proposed to simulate the flow in microtubes. The wall boundary condition combining the bounce-back and specular-reflection schemes is used to capture the slip velocity on the wall. Appropriate relation between the Knudsen number and relax-time constant is defined.

Findings – The computed-slip velocity, average velocity and non-linear pressure distribution along the microtube are in excellent agreement with analytical solution of the weakly compressible Navier-Stokes equations. The calculated-friction factors are also consistent with available experimental data. For simulations of slip flow in microtube, LBM is more accurate and efficient than DSMC method.

Research limitations/implications – The laminar flow in circular microtube is assumed to be axisymmetric. The present LBM is only applied to the simulation of slip flows ($0.01 < Kn_0 < 0.1$) in microtube.

Practical implications – Lattice-BGK method is a very useful tool to investigate the micro slip flows.

Originality/value – A revised axisymmetric D2Q9 lattice Boltzmann model is proposed to simulate the slip flow in axisymmetric microtubes.

Keywords Flow, Numerical analysis, Laminar flow, Fluid mechanics, Approximation theory

Paper type Research paper

1. Introduction

Micro-electro-mechanical-systems (MEMS) devices with dimensions ranging from 100 to 1 μ have found many applications in engineering and scientific researches (Gad-el-Hak, 1999). The fast development of these devices motivated the study of the fluid flow in MEMS (Arkilic *et al.*, 1997). MEMS are often operated in gaseous environments where the molecular mean free path of the gas molecules could be the same order as the typical geometric dimension of the device. Hence, the dynamics associated with MEMS can exhibit rarefied phenomena and compressibility effects (Arkilic *et al.*, 1997). Usually, the Knudsen number Kn are used to identify the effects. Kn is the ratio of the mean free path λ to the characteristic length L. Generally speaking, the continuum assumption for Navier-Stokes (NS) equations may break down if $Kn > 0.01$. For a flow case $0.01 < Kn < 0.1$, a slip velocity would appear in the wall boundary. The value of $0.1 < Kn < 10$ are associated with a transition flow regime. In the slip-flow regime, by introducing a slip velocity at the solid boundary the NS solver can still be used. In the transition regime, the conventional flow solver based on the NS equations is no longer applicable because the rarefaction effect is critical (Lim *et al.*, 2002).

International Journal of Numerical Methods for Heat & Fluid Flow
Vol. 17 No. 6, 2007
pp. 587-607

0961-5539
DOI 10.1108/09615530710761225

Many analytical studies of rarefied flow in microchannel have been carried out since the 1970s. An important analytical and experimental study of gaseous flow in two-dimensional (2D) microchannels was carried out by Arkilic *et al.* (1997). Through a formal perturbation expansion of the NS equations under an assumption of 2D isothermal flow, the study demonstrates the relative significance of the contribution of compressibility and rarefied effects and good agreements between the analytical and experimental studies were observed.

There are also some analytical studies about rarefied flow in circular microtubes. Analytical studies of Prud'homme *et al.* (1986) and Van den Berg *et al.* (1993) demonstrated non-constant pressure gradients but their analysis did not incorporate rarefied behavior and the analysis is only one-dimensional (1D) perturbation solution of the NS equations. Based on assumption of isothermal flow, Weng *et al.* (1999) obtained the analytical solution for rarefied gas flow in long-circular microtubes. Some experiments were also carried out to measure the friction constant $C = f^{*}Re$ in microtubes, which is not equal to 64 as the theoretical prediction for fully developed incompressible flow (Choi *et al.*, 1991; Yu *et al.*, 1995).

In addition to the above analytical and experimental investigations, there are many numerical studies on rarefied gas behavior in microchannel. Through introducing a slip velocity at the solid boundary, Beskok and Karniadakis (1993) presented numerical solutions of the NS and energy equations for flows with slight rarefaction. For simulations microflow, the direct simulation Monte Carlo method (DSMC) (Bird, 1994) are more popular because the approach is valid for the full range of flow regimes (continuum through free molecular). However, very large-computational effort is required in the DSMC simulations since the total number of simulated particles is directly related to the number of molecules.

Besides, numerical solution of NS equation and DSMC, the lattice Boltzmann method (LBM), which based on meso-scale level and has no continuum assumption, was also applied to simulate the microflows (Lim *et al.*, 2002; Nie *et al.*, 2002).

For LBM simulation micro flow, the boundary condition and correlating relax time τ with Kn are important. Nie *et al.* (2002) simulated a 2D-microchannel flow with bounce-back boundary treatment. However, in the study, a parameter to define Kn was obtained empirically. Lim *et al.* (2002) simulated microchannel flow and obtained good results with specular and extrapolation boundary treatments. They linked the τ with the molecular free-mean path λ by an assumption of $\lambda = \tau\delta x$. Succi (2002) and Tang *et al.* (2004) showed that a slip velocity on the wall can be captured by using a combination of the bounce-back and specular-reflection conditions. Although the value of the slip velocity may be highly dependent on the choice of the bounce-back probability b, the boundary condition is easy to implement. For simplicity, in our study, this boundary condition is applied to capture the correct velocity slip at the wall.

Previous LBM study of microflow is only concentrated in microchannel. Here, we would like to propose a revised axisymmetric LBM for axisymmetric flows in microtubes.

It is sure that 3D LBM can directly handle the axisymmetric flow problems (Huang *et al.*, 2006). However, for an axisymmetric flow problem, directly 3D simulation is not so efficient. To simulate the problem more efficiently, Halliday *et al.* (2001) proposed an axisymmetric D2Q9 model for the axisymmetric flow problems and it seems very successful for simulation steady flow in straight tube. The main idea of the model is inserting several spatial and velocity dependent "source" terms into the microscopic

evaluation equation for the lattice fluid's momentum distribution. However, it is found that some terms relative to the radial velocity are missing in the axisymmetric D2Q9 model of Halliday *et al.* (2001) and later-developed model (Lee *et al.*, 2005). Although the terms may not affect simulations of the flows in straight circular pipe, they would lead to large error for simulation the constricted or expanded pipe flows.

The main aim of the present paper is to derive a correct D2Q9 axisymmetric model to numerically investigate the flow in microtubes. We also would like to compare the accuracy and efficiency between the LBM and the DSMC when simulate the slip flow in microtubes.

The structure of this paper is as follows. Firstly, a revised axisymmetric LBM is proposed and the implementation of the LBM and boundary condition is discussed. Then the LBM is applied to simulate the slip flow in microtubes for cases $Kn = 0.1, 0.05, 0.025$ with different inlet/outlet pressure ratio. The slip velocity, bulk velocity and pressure distribution along the tube are compared with analytical solution (Weng *et al.*, 1999) in detail. The friction factors are compared with the available experimental data. Finally, the efficiency and accuracy comparisons between DSMC and LBM are carried out.

2. LBM model and boundary condition

2.1 LBM model

In this part, an axisymmetric D2Q9 model is proposed to simulate the axisymmetric flows in a long microtube. The derivation of our model is illustrated in Appendix 1.

Here, we consider the problems of the laminar internal flow of a weakly compressible, isothermal flow in circular pipe with an axis in x direction. The geometry is shown in Figure 1. For the axisymmetric flow, the azimuthal velocity u_φ and φ coordinate derivatives vanish from the continuity and NS equations. The full 2D time-invariant constant viscosity NS equations for a compressible fluid, ignoring body force, are (in the pseudo-Cartesian coordinates (x, r)):

$$\rho\left(u\frac{\partial u}{\partial x}+v\frac{\partial u}{\partial r}\right)=-\frac{\partial p}{\partial x}+\mu\left[\frac{\partial^2 u}{\partial x^2}+\frac{1}{r}\frac{\partial u}{\partial r}+\frac{\partial^2 u}{\partial r^2}+\frac{1}{3}\frac{\partial}{\partial x}\left(\frac{\partial u}{\partial x}+\frac{\partial v}{\partial r}+\frac{v}{r}\right)\right] \quad (1)$$

$$\rho\left(u\frac{\partial v}{\partial x}+v\frac{\partial v}{\partial r}\right)=-\frac{\partial p}{\partial r}+\mu\left[\frac{\partial^2 v}{\partial x^2}+\frac{1}{r}\frac{\partial v}{\partial r}+\frac{\partial^2 v}{\partial r^2}-\frac{v}{r^2}+\frac{1}{3}\frac{\partial}{\partial r}\left(\frac{\partial u}{\partial x}+\frac{\partial v}{\partial r}+\frac{v}{r}\right)\right] \quad (2)$$

The continuity equation is given by:

$$\frac{\partial \rho u}{\partial x}+\frac{\partial \rho v}{\partial r}+\frac{\rho v}{r}=0 \quad (3)$$

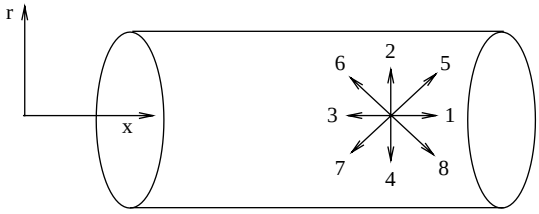

Figure 1.
Geometry of circular tube and LBM D2Q9 model

The equation of state for an ideal gas is given by:

$$p = \rho RT \tag{4}$$

In above equations, u and v are the stream-wise and wall-normal components of velocity $\mathbf{u}$, μ is the molecular viscosity, ρ is the density, p is the pressure and R is the specific gas constant. In equations (1) and (2), we have assumed a Stokes continuum hypothesis for the second coefficient of viscosity (Landau and Lifschitz, 1987).

Our present axisymmetric D2Q9 model is proposed to simulate the microtube flows described by above equations. Among different lattice Boltzmann equation (LBE) models in application, the lattice Bhatnagar-Gross-Krook (LBGK) model is the simplest one because it only has one scalar relaxation parameter and a simple equilibrium momentum distribution function. Here, our axisymmetric LBM is derived from LBGK D2Q9 model. In our axisymmetric D2Q9 model, the nine discrete velocities of our model are defined as following:

$$\mathbf{e}_i = \begin{cases} (0,0) & i = 0 \\ (\cos[(i-1)\pi/2], \sin[(i-1)\pi/2])c & i = 1,2,3,4 \\ \sqrt{2}(\cos[(i-5)\pi/2+\pi/4], \sin[(i-5)\pi/2+\pi/4])c & i = 5,6,7,8 \end{cases} \tag{5}$$

where $c = \delta_x/\delta_t$, and in our studies $c = 1$. δ_x and δ_t are the lattice spacing and time step size, respectively.

In our model, $f_i(x, r, t)$ is the distribution function for particles with velocity $\mathbf{e}_i$ at position (x, r) and time t. The macroscopic density ρ and momentum $\rho\mathbf{u}$ are defined as:

$$\sum_{i=0}^{8} f_i = \rho, \quad \sum_{i=0}^{8} f_i e_{i\alpha} = \rho u_\alpha \tag{6}$$

The equilibrium distribution f_i^{eq} of D2Q9 model (Qian *et al.*, 1992) is defined by equation (7):

$$f_i^{\mathrm{eq}}(x,r,t) = \omega_i \rho \left[1 + \frac{\mathbf{e}_i \cdot \mathbf{u}}{c_s^2} + \frac{(\mathbf{e}_i \cdot \mathbf{u})^2}{2c_s^4} - \frac{\mathbf{u}^2}{2c_s^2}\right] \quad i = 0,1,2,\ldots,8 \tag{7}$$

where, $c_s = c/\sqrt{3}$, $\omega_0 = 4/9$, $\omega_i = 1/9, (i = 1,2,3,4)$, $\omega_i = 1/36, (i = 5,6,7,8)$.

The two main steps of lattice BGK model are collision and streaming. In the collision step, a group of calculations (8) and (9) are implemented:

$$f_i^{\mathrm{ne}} = f_i(x,r,t) - f_i^{\mathrm{eq}}(x,r,t) \tag{8}$$

$$f_i^{+}(x,r,t) = f_i^{\mathrm{eq}}(x,r,t) + \left(1 - \frac{1}{\tau}\right) f_i^{\mathrm{ne}} + \delta_t h_i^{(1)} + \delta_t^2 h_i^{(2)} \tag{9}$$

In above equations, f_i^{ne} is the non-equilibrium part of distribution function. f_i^{+} is the post-collision distribution function. $h_i^{(1)}$ and $h_i^{(2)}$ are the "source" terms added into the collision step, which can be calculated through below equations (10) and (11), respectively. The brief derivation of the equations is illustrated in Appendix 1:

$$h_i^{(1)} = \frac{-\omega_i \rho u_r}{r} \tag{10}$$

$$h_i^{(2)} = \frac{\omega_i}{2r}\left(\partial_r \frac{\rho}{3} + \partial_x \rho u_x u_r + \partial_r \rho u_r u_r\right) + \frac{3\omega_i \rho \nu}{r}(e_{ix}\partial_r u_x + e_{ir}\partial_r u_r) - \frac{3\omega_i \rho \nu}{r^2} u_r e_{ir} - 3\omega_i \rho\left(\frac{u_x u_r}{r} e_{ix} + \frac{u_r u_r}{r} e_{ir}\right) - (1-\tau)\omega_i\left(\frac{1}{r}\partial_x \rho u_r e_{ix} - \frac{\rho u_r}{r^2} e_{ir} + \frac{\partial_r \rho u_r}{r} e_{ir}\right) \tag{11}$$

In above formulas, the relax time constant τ and the fluid kinetic viscosity ν satisfies the below equation:

$$\nu = c_s^2 \delta_t (\tau - 0.5) \tag{12}$$

For the microflow simulation, the τ should be related to the Knudsen number.

In the streaming step, the new distribution function value obtained from equation (9) would propagate to neighbour eight lattices. That procedure can be represented by the following equation (13):

$$f_i(x + e_{ix}, \delta t, r + e_{ir}, \delta t, t + \delta t) = f_i^+(x, r, t) \tag{13}$$

For the velocity derivations in equation (11), the terms $\partial_r u_x + \partial_x u_r$, $\partial_x u_x$ and $\partial_r u_r$ can all be obtained through equation (14) with $\alpha = x, \beta = r$; $\alpha = \beta = x$; $\alpha = \beta = r$, respectively:

$$\begin{aligned} \rho\nu(\partial_\beta u_\alpha + \partial_\alpha u_\beta) &= -\left(1 - \frac{1}{2\tau}\right)\sum_{i=0}^{8} f_i^{(1)} e_{i\alpha} e_{i\beta} \\ &= -\left(1 - \frac{1}{2\tau}\right)\sum_{i=0}^{8} f_i^{\mathrm{ne}} e_{i\alpha} e_{i\beta} + o(\varepsilon^2) \end{aligned} \tag{14}$$

For the term $\partial_r u_x$ in equation (11), it is equal to $(\partial_r u_x + \partial_x u_r) - \partial_x u_r$. Since, $(\partial_r u_x + \partial_x u_r)$ can be easily obtained by equation (14), only value of $\partial_x u_r$ is left unknown to determine $\partial_r u_x$. Here, we recourse to finite difference method to obtain $\partial_x u_r$ at lattice node (i, j), which can be calculated by equation (15):

$$(\partial_x u_r)_{i,j} = \frac{(u_r)_{i+1,j} - (u_r)_{i-1,j}}{2\delta_x} \tag{15}$$

The values of $\partial_r u_x + \partial_x u_r$, $\partial_x u_x$, $\partial_r u_r$, $\partial_r u_x$ and $\partial_x u_r$ for the lattice nodes which just on the wall boundary can also be calculated from equations (14) and (15). Obtaining these values for lattice nodes on the periodic boundary is also easy. However, to obtain these values for the nodes on the inlet/outlet pressure-specified boundary, these values are extrapolated from those of the inner nodes.

2.2 Knudsen number and boundary condition

Correlating the parameter τ with *Kn* is important for LBM application in simulation micro-flows. (Nie *et al.*, 2002; Tang *et al.*, 2004) Here, an expression (Tang *et al.*, 2004) between *Kn* and τ which based on the gas kinematics is used in our simulation but we derived it in a simpler way in the following.

Form the kinetic theory of gases, the density can be determined by:

$$\rho = \frac{mp}{k_B T} \tag{16}$$

where m represents the molecular mass and k_B is the Boltzmann constant. On the other hand, in LBM, the density and pressure have the relationship (Qian *et al.*, 1992):

$$\rho = \frac{p}{c_s^2} \tag{17}$$

Hence, in LBM, we have:

$$\frac{k_B T}{m} = c_s^2 \tag{18}$$

For an ideal gas modeled as rigid spheres, the mean free path λ is related to the viscosity ν as:

$$\nu = 0.5 \nu_m \lambda \tag{19}$$

where the mean velocity of the molecular $v_m = \sqrt{8K_{\mathrm{B}}T/\pi m}$. Hence, form equations (12) and (19), we get:

$$Kn = \frac{\lambda}{D} = \frac{2\nu}{v_m D} = \sqrt{\frac{\pi}{6}} \frac{(\tau - 0.5)}{N_D} \quad \text{or} \quad \tau = \frac{KnN_D}{\sqrt{\pi/6}} + 0.5 \tag{20}$$

where N_D is the lattice number in the tube diameter, Kn is local Knudsen number. Since, the mean free path is inversely proportional to the pressure, the local Kn can be calculated by:

$$Kn = \frac{Kn_{\mathrm{o}} p_{\mathrm{o}}}{p(x, r)} \tag{21}$$

where Kn_{o} and p_{o} are the Kn and the pressure at the outlet. So, in equation (20), τ is variable along the microtube and the corresponding ν can be obtained from equation (12).

Another important issue about using LBM to simulate the micro flows is wall boundary condition. For wall boundary condition, bounce-back scheme is usually used to realize non-slip boundary condition when simulate continuum flow. On the other hand, specular reflection scheme (Lim *et al.*, 2002) can be applied to free-slip boundary condition where no momentum is to be exchanged with the wall along the tangential component. For real gas flow in microtubes, a combination of the two schemes is considered here. To describe boundary condition treatment, a wall $\partial\Omega$ is completely specified. For a point $\mathbf{x}(\mathbf{x} \in \partial\Omega)$, $\mathbf{n}$ is the inward unit normal vector of the wall. After streaming step implemented, the unknown distribution functions of $f_i(\mathbf{x}, t)$, $\boldsymbol{e}_i \cdot \mathbf{n} > 0$, can be evaluated by Succi (2002) and Tang *et al.* (2004):

$$f_i(\mathbf{x}, t) = b f_j(\mathbf{x}, t) + (1 - b) f_k(\mathbf{x}, t) \tag{22}$$

where f_j(**x**,t) is the distribution function in $\mathbf{e}_j$ direction, where $\mathbf{e}_i - \mathbf{e}_j = 2\mathbf{e}_i$, and $f_k(\mathbf{x}, t)$ is the distribution function in $\mathbf{e}_k$ direction, where $\mathbf{e}_i - \mathbf{e}_k = 2\mathbf{n}$. b is the bounce-back probability chosen as 0.7.

For the inlet/outlet boundary conditions, the pressure is specified and the corresponding velocity value in these boundaries is extrapolated from the next inner nodes (Fang *et al.*, 2002). Hence, the equilibrium part of distribution function can be determined and the non-equilibrium part of distribution function can be obtained through extrapolation (Fang *et al.*, 2002). So, the collision step for boundary nodes can be implemented normally as inner nodes.

The axisymmetric boundary condition is also applied in most simulations here. In most simulations, the computational domain is an axisymmetric plane above the axis. To implement this boundary condition, an extra row of grids below the axis is added. The variables in the grid of this row can be evaluated from that of its symmetric node. For example, if $j = 2$ and $j = 1$ represents the row index of the axis and the extra row, velocities in the extra grids can be obtained by $(u_x)_{i,1} = (u_x)_{i,3}, (u_r)_{i,1} = (-u_r)_{i,3}$, and the corresponding source terms in equations (10) and (11) can be evaluated as $(h)_{i,1} = (h)_{i,3}$. In this way, the collision and streaming steps for lattices in the extra row can be implemented as that of inner lattices.

3. Results and discussion

3.1 Distributions of pressure and velocity

In our simulation, the radius is represented by 11 lattice nodes (ten lattice space) and the length of the tube is 20 times of the diameter except for specially noted cases. In all of cases, the Mach number in tube is very low. Even for case of $Pr = 3.0$, maximum Mach number in tube is $M = 0.15/c_s \ll 1$, which satisfy the requirement of our axisymmetric D2Q9 model. The stream-wise momentum accommodation coefficient $\sigma = 1$ has been used for almost all engineering calculations (Weng *et al.*, 1999). Therefore, we take $\sigma = 1$ throughout the paper.

Figures 2 and 3 show the axial and radial-velocity distribution along the tube ($Pr = 2, Kn_o = 0.1$), respectively. The u, v velocity contour are also shown in Figures 2 and 3, respectively. From the Figure 2, we can see that the axial-velocity profile is parabolic type and the slip velocity at the wall and the central velocity increase toward the exit. Owing to the pressure decreasing, the density of gas also decreases along the tube. To satisfy mass conservation, the average velocity must increase toward the exit. In Figure 3, the magnitude of the radial velocity is much smaller than that of axial velocity. These results are consistent with previous studies on microchannel (Arkilic *et al.*, 1997; Lim *et al.*, 2002).

The pressure distribution along the tube predicted from the first slip boundary condition is illustrated in equation (23), which is originally given by Weng *et al.* (1999). The derivation of present expression is illustrated in Appendix 2:

$$\tilde{p}(\tilde{x}) = -8Kn_o + \sqrt{(8Kn_o)^2 + (1 + 16Kn_o)\tilde{x} + (Pr^2 + 16Kn_oPr)(1 - \tilde{x})} \qquad (23)$$

In equation (23), $\tilde{p}$ is the pressure normalized by outlet pressure, $\tilde{x} = x/L$, L is the tube length. Pr is the ratio of the inlet and outlet pressure.

The pressure drop along the tube which deviate from linear pressure drop for different Pr with the same outlet Knudsen number $Kn_o = 0.1$ are shown in Figure 4. When Pr increase, the compressibility effect within the tube is also increase, results in a larger deviation from the linear pressure distribution. In Figure 4, our results agree well with equation (23).

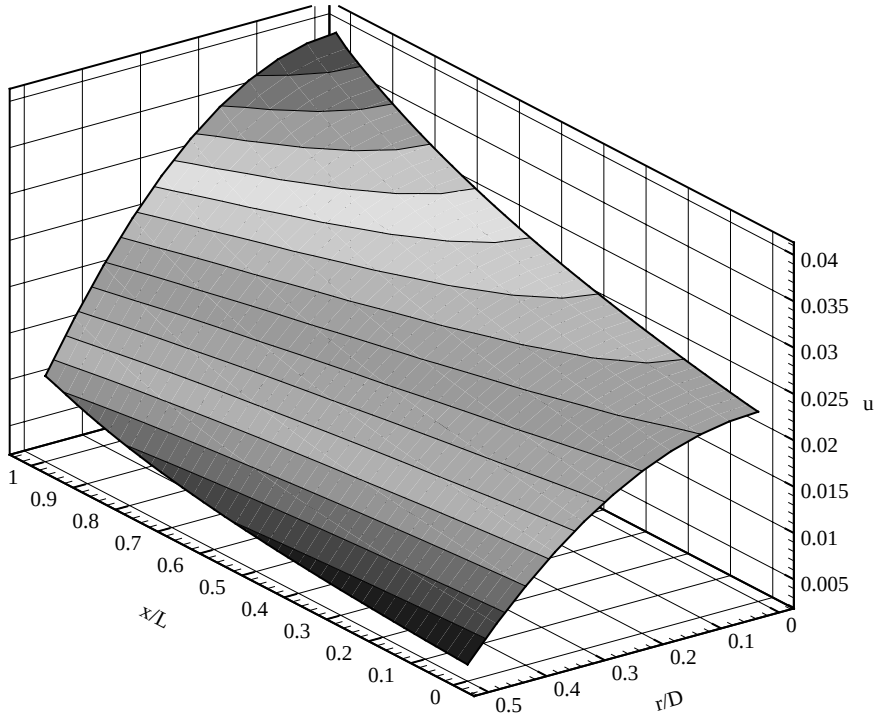

Figure 2.
Axial-velocity distributions in the tube

The pressure drops along the tube for different outlet Kn_o are shown in Figure 5. Compared with the analytical solution equation (23), the results of LBM is quite good. Figure 5 shows that the larger Kn_o, the smaller the deviation from the linear-pressure distribution. It seems that the rarefaction effect (indicate by Kn_o) can decrease the curvature in the pressure distribution which caused by the compressibility effect. Maybe that means the compressibility effect and the rarefaction effect on the pressure distribution are contradictory.

The Knudsen numbers along the stream-wise direction are shown in Figure 6. Kn is a function of the local pressure. With the decreasing pressure along the tube, the Knudsen number increases and reaches its maximum value at the outlet. For different outlet Kn_o, the slope of Kn curve along the tube is different. For smaller Kn_o, the slope of Kn curve is smaller although Pr is same.

In Figure 7, the variation of slip velocity along the microtube wall is shown. Firstly, we obtained the analytical solution of slip velocity from results of Weng *et al.* (1999) (Appendix 2). Equation (B2) is can be normalized by the central velocity at outlet U_{oc}:

$$\frac{U(x,r)}{U_{oc}} = \frac{\mathrm{d}\tilde{p}/\mathrm{d}\tilde{x}}{(\mathrm{d}\tilde{p}/\mathrm{d}\tilde{x})_o} \frac{(0.25 + Kn - r^2/D^2)}{(0.25 + Kn_o)} \tag{24}$$

where $\mathrm{d}\tilde{p}/\mathrm{d}\tilde{x}$ is the non-dimensional pressure gradient and the $(\mathrm{d}\tilde{p}/\mathrm{d}\tilde{x})_o$ means the pressure gradient at exit, which can be referred to equation (B7) in Appendix 2.

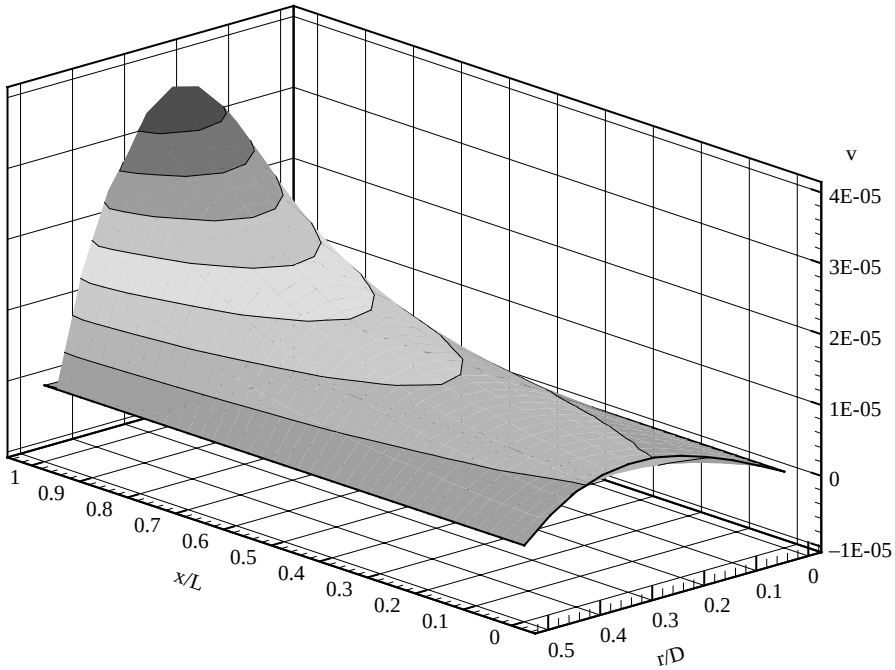

Figure 3.
Radial-velocity distributions along the tube

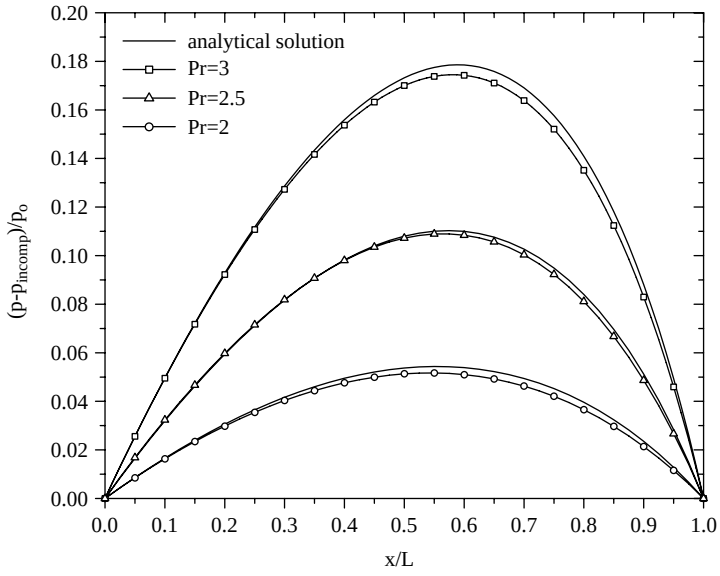

Figure 4.
Pressure distribution along the tube for different Pr ($Kn_o = 0.1$)

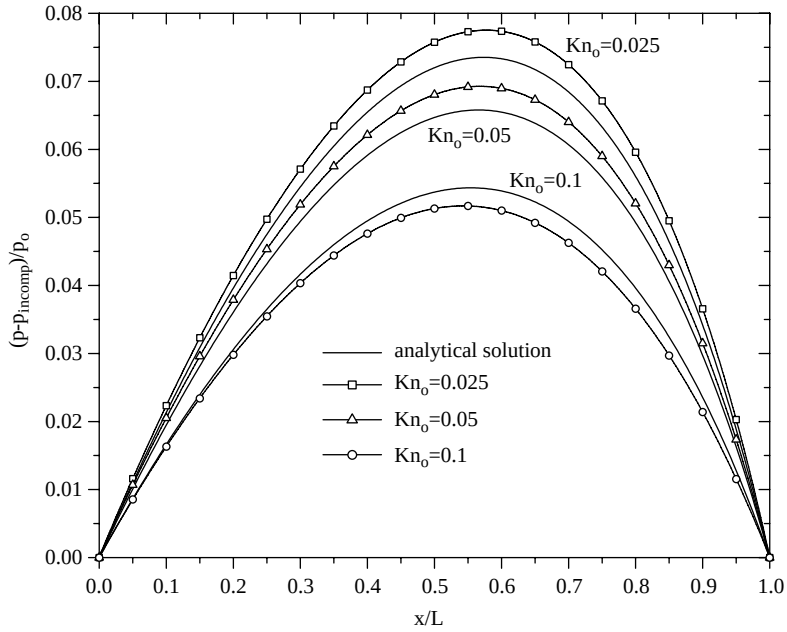

Figure 5.
Pressure distribution along the tube for different Knudsen number ($Pr = 2$)

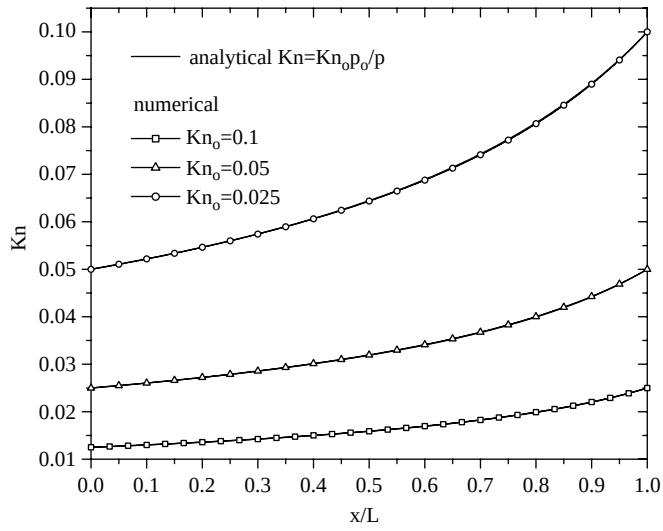

Figure 6.
Local Kn distribution along the tube for different Kn_o ($Pr = 2$)

Hence, the analytical solution for slip velocity on the wall and average velocity in microtube are equations (25) and (26), respectively:

$$\frac{U_{\text{slip}}(x)}{U_{oc}} = \frac{\mathrm{d}\tilde{p}/\mathrm{d}\tilde{x}}{(\mathrm{d}\tilde{p}/\mathrm{d}\tilde{x})_{\text{o}}} \frac{Kn}{(0.25 + Kn_{\text{o}})} \tag{25}$$

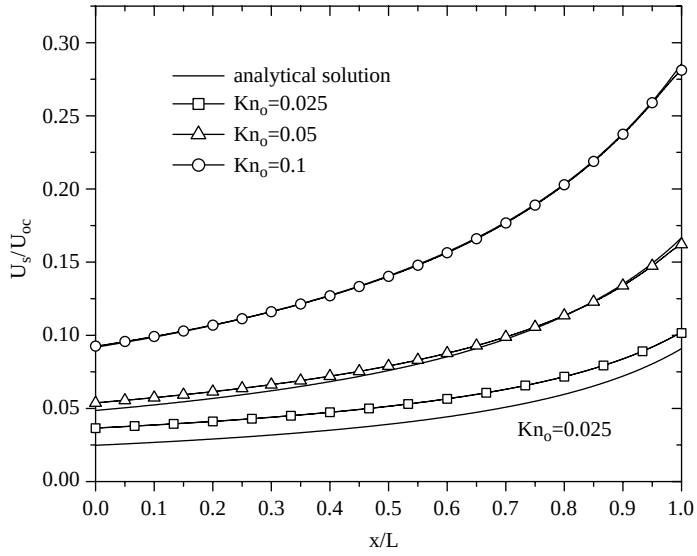

Figure 7.
Slip velocity in wall along the tube for different Kn_o ($Pr = 2$)

$$\frac{U_{av}(x)}{U_{oc}} = \frac{d\tilde{p}/d\tilde{x}}{(d\tilde{p}/d\tilde{x})_o} \frac{(1/8 + Kn)}{(1/4 + Kn_o)} \tag{26}$$

From equation (25), we can see that since the local Knudsen number increases and the slope of pressure drop also increases along the tube, the slip velocity on the wall would increase along the microtube. Figure 8 shows the average velocity variations along the stream-wise direction. The average velocity increases as the flow proceeds down the tube since density decrease along the microtube. In Figures 7 and 8, both the slip

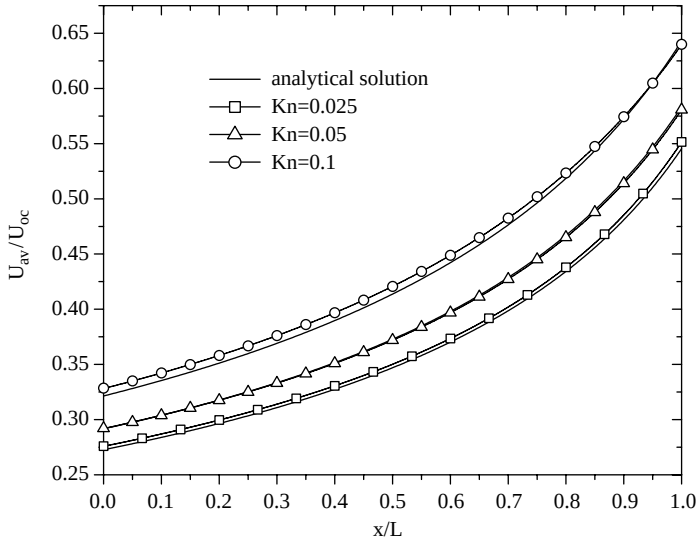

Figure 8.
Average axial velocity U_{av} along the tube for different Kn_o ($Pr = 2$)

velocity on wall and local bulk velocity along the microtube agree well with the analytical solution equations.

3.2 Mass flow rate and normalized friction constant

The effect of rarefaction on mass flow rate is investigated by comparison of the LBE result with analytical predictions. The non-dimensional mass flow rate $\tilde{Q}$ can be expressed as a function of pressure ratio (Appendix 2):

$$\tilde{Q} = \frac{\dot{q}}{(\dot{q})_{\text{continuum}}} = 1 + \frac{16Kn_o}{Pr + 1} \tag{27}$$

In Figure 9, the non-dimensional mass flow rate computed by the LBE method for $Kn_o = 0.1$ is compared with the first order analytical prediction equation (27). For all cases, slip effects become less pronounced with increasing pressure ratio. The LBE results agree well with analytical results and the deviation is less than 4 percent.

Then in Figure 10, the friction factors predicted by present LBM simulations are compared with experimental results of Kim *et al.* (2000). The theoretical friction constant ($C_0 = f^*Re = 64$) for fully developed incompressible flow is used to normalize friction constant $C = f^*Re$. The microtubes used in the experiment are also shown in Figure 10. Here, our numerical data were taken from results of cases $Kn_o = 0.013$ with different inlet/outlet pressure ration. In these cases, for $Kn = \lambda/D = 0.013$, the corresponding simulated diameters D of microtubes for Nitrogen, Argon and Helium are listed in Table I. The diameters of our simulation are all close to that of corresponding experimental facility. Hence, our numerical results are valid to compare with the experimental data. In Figure 10, the normalized friction constant C^* obtained by LBM ranges from 0.80 to 0.86, which agree well with the experiment data.

Besides, experiment of Kim *et al.* (2000) and Choi *et al.* (1991) also found that for nitrogen flow in microtube with diameters smaller than 10 μm, $C = f^*Re = 53$. Another experiment conducted by Yu *et al.* (1995) concluded that $C = f^*Re = 50.13$

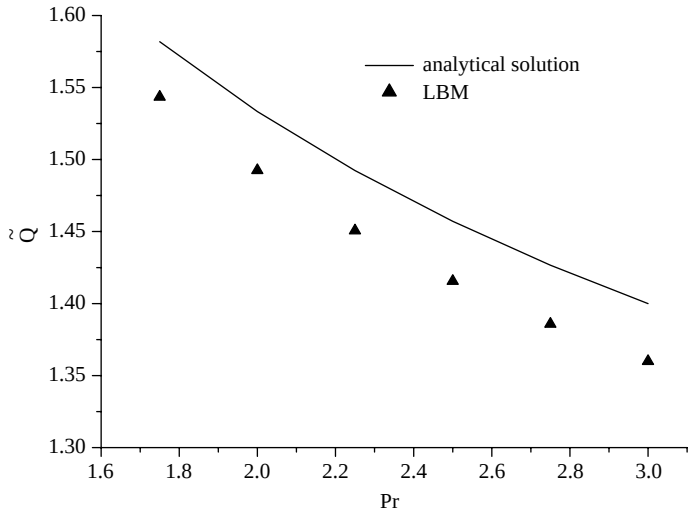

Figure 9.
Mass flow rate normalized to non-slip mass flow rate as a function of Pr at $Kn_o = 0.1$

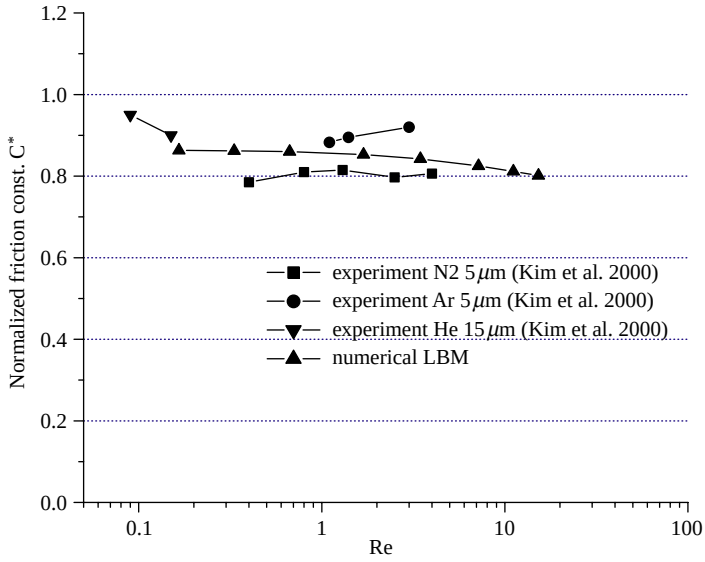

Figure 10.
Normalized friction constant C^* of gas flow in microtube as a function of Re ($Kn_o = 0.013$)

Gas (10^5 Pa)	Nitrogen	Argon	Helium
Mean free path (nm)	67	72	196
Diameter of tube (μm)	5.2	5.5	15.0

Table I.
Simulated diameter of microtubes for different gas flow ($Kn_o = 0.013$)

for laminar nitrogen flow in microtubes with diameter 19 μm. In Figure 10, it was observed that our numerical data are also in consistent with their experimental results (Choi *et al.*, 1991; Yu *et al.*, 1995).

3.3 Comparison with DSMC

To demonstrate the efficiency of the LBM, we compared the accuracy and efficiency of the LBM and DSMC. It is well known that DSMC is the most popular model for simulation of micro flows. DSMC is a particle-based method proposed by Bird (1994). Unlike the molecular dynamics (MD) method which takes each individual molecule into consideration, DSMC method assumes that a group of molecules have the same properties such as velocity and temperature which can be obtained by statistical analysis. In this way, the computational effort can be greatly reduced compared with the MD method (Bird, 1976; Bird, 1994). Here, the developed DSMC code (Mao *et al.*, 2003) was used to simulate the slip flow in microtubes.

In the DSMC simulation, the working gas is nitrogen. The physical geometry is 200 μm long and radius of the tube is 2.5 μm. The computational region is an axisymmetric plane divided into 400 $\times$ 30 sampling cells and each cell contains four subcells. The total number of simulated particles is about 4.8×10^5. That means nearly 40 particles in a sampling cell (Mao *et al.*, 2003). In this part, the case of $Kn_o = 0.0134$ and $Pr = 2.5$ was simulated.

In the LBM simulation, the uniform square lattices 801 × 21 is used to simulate the same microtube flow. For this case, if the computational domain is an axisymmetric plane and the axisymmetric boundary condition is applied, the calculation is unstable. However, when the computational domain is a whole plane passing through the axis, the calculation is stable with the slip wall boundary condition. Hence, here the computational domain is a whole plane passing through the axis and the diameter is represented by 21 lattice nodes.

The present DSMC and LBM calculations were performed on a single-CPU of the computer Compaq ES40 supercomputer. To make the efficiency comparison, the same convergence criterion was set as:

$$\sum_i \frac{\|\mathbf{u}(\mathbf{x}_i, t) - \mathbf{u}(\mathbf{x}_i, t-1)\|}{\|\mathbf{u}(\mathbf{x}_i, t)\|} < 10^{-6} \tag{28}$$

The velocity field error is measured by θ which is defined as:

$$\theta = \frac{\sum_i (u(r_i) - u_a(r_i))^2}{\sum_i u_a^2(r_i)} \tag{29}$$

where $u_a(r_i)$ is the analytical solution obtained by Weng *et al.* (1999) and r_i is the mesh point at intersection $x/L = 0.375$ where the microflow is supposed to be in fully developed region.

The efficiency and accuracy comparison is listed in Table II. The mesh or cell number is comparable for LBM and DSMC simulations. However, since DSMC still has to simulate 4.8×10^5 particles, it used much larger memory than LBM in the simulation. To obtain the well-converged results, DSMC takes more CPU time than LBM.

The velocity profiles at intersection $x/L = 0.375$ obtained by analytical solution (Weng *et al.*, 1999), LBM and DSMC are shown in Figure 11. The velocity U is normalized by outlet U_{oc} r is normalized by the diameter. Compared with the analytical solution, the result of LBM seems more accurate than that of DSMC.

4. Conclusion

In this paper, a revised axisymmetric D2Q9 model was applied to investigate gaseous slip flow with slight rarefaction through long microtubes. With limit of small Mach number, this axisymmetric LBGK model successfully recovered the weakly compressible NS equation in the cylindrical coordinates through Chapman Enskog expansion (refer to the Appendix 1). For the additional source term in our model, most velocity gradient terms can be obtained from high order momentum of distribution function, which is consistent with the philosophy of the LBM. For the slip wall boundary condition, the wall boundary condition combined the bounce-back and specular-reflection scheme was applied for microtube flows with Kn_o in range (0.01, 0.1).

Table II.
Efficiency and accuracy comparison (LBM and DSMC) ($Kn_o = 0.0134$, $Pr = 2.5$)

Method	CPU time (s)	Mesh or cells	Memory (M)	θ
LBM	4.52×10^2	1.6×10^4	9.2	4.31×10^{-4}
DSMC	3.22×10^4	1.2×10^4	31.4	3.3×10^{-3}

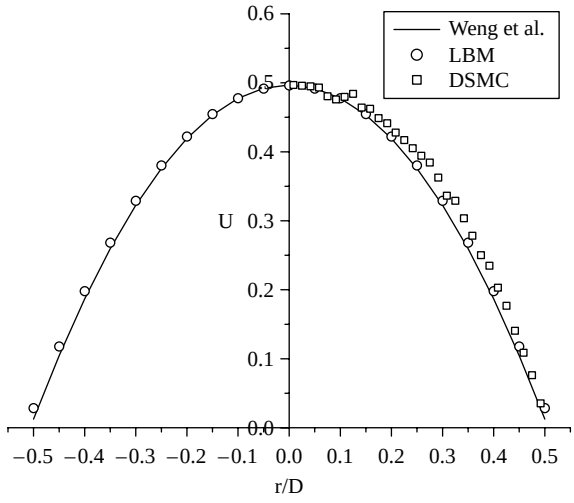

Figure 11.
Velocity profiles at $x/L = 0.375$ obtained by analytical solution, LBM and DSMC

The distributions of pressure, the slip velocity and the average velocity along the microtube all agree well with the analytical results. The friction factors are compared with experimental results and good agreements are also observed. The axisymmetric LBGK model was successfully applied to simulate the laminar flow in microtubes.

Through comparison, it was found that our LBM is more accurate and efficient than DSMC when simulate the slip flow in microtube. Although present LBM is only applied to the slip flow simulation ($0.01 < Kn_0 < 0.1$) in microtube, the LBM may be extended to study the transition flow or higher Knudsen number cases in the future.

References

Arkilic, E.B., Schmidt, M.A. and Breuer, K.S. (1997), "Gaseous slip flow in long micro-channels", *J. MEMS*, Vol. 6 No. 2, pp. 167-78.

Beskok, A. and Karniadakis, G. (1993), "Simulation of heat and momentum transfer in micro-geometries", AIAA Paper 93-3269.

Bird, G.A. (1976), *Molecular Gas Dynamics*, Clarendon, Oxford.

Bird, G.A. (1994), *Molecular Gas Dynamics and the Direct Simulation of Gas Dynamics*, Clarendon, Oxford.

Choi, S.B., Barron, R. and Warrington, R. (1991), "Fluid Flow and heat transfer in microtubes", *Micromechanical Sensors, Actuator and Systems, ASME DSC*, Vol. 32, pp. 123-34.

Fang, H.P., Wang, Z.W., Lin, Z.F. and Liu, M.R. (2002), "Lattice Boltzmann method for simulating the viscous flow in large distensible blood vessels", *Physical Review E*, Vol. 65, 051925.

Gad-el-Hak, M. (1999), "The fluid mechanics of microdevices-the Freeman scholar lecture", *J. Fluids Eng.*, Vol. 121 No. 1, pp. 5-33.

Halliday, I., Hammond, L.A., Care, C.M., Good, K. and Stevens, A. (2001), "Lattice Boltzmann equation hydrodynamics", *Phys. Rev. E*, Vol. 64, 011208.

He, X. and Luo, L. (1997), "Lattice Boltzmann model for the incompressible Navier-Stokes equation", *J. Stat. Phys.*, Vol. 88 Nos 3/4, pp. 927-43.

Huang, H., Lee, T.S. and Shu, C. (2006), "Lattice-BGK simulation of steady flow through vascular tubes with double constrictions", *Int. J. Num. Methods for Heat & Fluid Flow*, Vol. 16 No. 2, pp. 185-203.

Kim, M.S., Araki, T., Inaoka, K. and Suzuki, K. (2000), "Gas flow characteristic in microtubes", *JSME International Journal Series B, Fluid and Thermal Engineering*, Vol. 43 No. 4, pp. 634-9.

Landau, L.D. and Lifschitz, E.M. (1987), *Fluid Mechanics*, 2nd ed., Pergamon, Oxford.

Lee, T.S., Huang, H. and Shu, C. (2005), "An axisymmetric incompressible Lattice-BGK model for simulation of the pulsatile flow in a circular pipe", *Int. J. Numer. Meth. Fluids*, Vol. 49 No. 1, pp. 99-116.

Lim, C.Y., Shu, C., Niu, X.D. and Chew, Y.T. (2002), "Application of lattice Boltzmann method to simulate microchannel flows", *Phys. Fluids*, Vol. 14 No. 7, pp. 2299-308.

Mao, X.H., Shu, C. and Chew, Y.T. (2003), "Numerical and theoretical study of a micro tube flow", *Int. J. Nonlinear Sciences and Numer. Simulation*, Vol. 4 No. 2, pp. 187-200.

Nie, X., Doolen, G.D. and Chen, S.Y. (2002), "'Lattice Boltzmann simulation of fluid flows in MEMS", *J. Stat. Phys.*, Vol. 107, pp. 279-89.

Prud'homme, R., Chapman, T. and Bowen, J. (1986), "Laminar compressible flow in a tube", *Appl. Sci. Res.*, Vol. 43, pp. 67-74.

Qian, Y.H., d'Humieres, D. and Lallemand, P. (1992), "Lattice BGK models for Navier-Stokes equation", *Europhys. Lett.*, Vol. 17, pp. 479-84.

Succi, S. (2002), "Mesoscopic modeling of slip motion at fluid-solid interfaces with heterogeneous catalysis", *Phys. Rev. Lett.*, Vol. 89 No. 6, 064502.

Tang, G.H., Tao, W.Q. and He, Y.L. (2004), "Lattice Boltzmann method for simulating gas flow in microchannels", *Int. J. Mod. Phys. C*, Vol. 15 No. 2, pp. 335-47.

Van den Berg, H., Tenseldam, C. and VanderGulik, P. (1993), "Compressible laminar flow in a capillary", *J. Fluid Mech.*, Vol. 246, pp. 1-20.

Weng, C.I., Li, W.L. and Hwang, C.C. (1999), "Gaseous flow in microtubes at arbitrary Knudsen numbers", *Nanotechnology*, Vol. 10, pp. 373-9.

Yu, D., Warrington, R., Barron, R. and Ameel, T. (1995), "An experimental and theoretical investigation of fluid flow and heat transfer in Microtubes", *ASME/JSME Thermal Engineering Conference*, Vol. 1, pp. 523-30.

Appendix 1. Brief derivation of the axisymmetric model

Here, we would show how continuity equation (A1) and momentum equation (A2) in the pseudo-Cartesian coordinates (x, r) can be recovered from our axisymmetric D2Q9 model:

$$\frac{\partial \rho}{\partial t} + \frac{\partial \rho u_\beta}{\partial x_\beta} = -\frac{\rho u_r}{r} \tag{A1}$$

$$\frac{\partial \rho u_\alpha}{\partial t} + \frac{\partial \rho u_\beta u_\alpha}{\partial x_\beta} + \frac{\rho u_\alpha u_r}{r} + \frac{\partial p}{\partial x_\alpha} - \mu \frac{\partial^2 u_\alpha}{\partial x_\beta^2} - \mu \partial_\alpha (\nabla \cdot \mathbf{u}) = \frac{\mu}{r}\left(\frac{\partial u_\alpha}{\partial r} - \frac{u_r}{r}\,\delta_{\alpha r}\right) \tag{A2}$$

where $\nabla \cdot \mathbf{u} = \partial_\beta u_\beta + u_r/r$. Here, we adopt the Einstein convention that the same index appears twice in any term, summation over the range of that index is implied. u_α, u_β is the velocity $u_x$or u_r. α, β is x or r, x_α, x_β means x or r.

It is noticed that the small discrepancy between equations (1), (2) and equation (A2) is the coefficient before term $\nabla \cdot \mathbf{u}$, in equation (1) that is 1/3, here in equation (A2) is unit.

Since, we consider a slight rarefaction in long microtubes, which means the weakly compressible flow, this term $\nabla \cdot \mathbf{u}$ should be very small. The coefficient difference can be neglected. Our numerical results also verified this opinion.

To recover above equations, the Chapman-Enskog expansion is applied. The evaluation equation to describe 2D flow in (x, r) pseudo-Cartesian coordinates is illustrated as equation (A3):

$$f_i(x + e_{ix}\delta_t, r + e_{ir}\delta_t, t + \delta_t) - f_i(x, r, t) = \frac{1}{\tau}\left[f_i^{\mathrm{eq}}(x, r, t) - f_i(x, r, t)\right] + h_i(x, r, t) \tag{A3}$$

equation (A3) is similar to the evaluation equation in 2D (x, y) Cartesian coordinates except that a source term $h_i(x, r, t)$ was incorporated into the microscopic evaluation equation (Halliday *et al.*, 2001).

Here, we introduce the following expansions (He and Luo, 1997):

$$f_i(x + e_{ix}\delta_t, r + e_{ir}\delta_t, t + \delta_t) = \sum_{n=0}^{\infty} \frac{\varepsilon^n}{n!} D^n f_i(x, r, t) \tag{A4}$$

$$\begin{cases} f_i = f_i^{(0)} + \varepsilon f_i^{(1)} + \varepsilon^2 f_i^{(2)} + \cdots \\ \partial_t = \varepsilon\partial_{1t} + \varepsilon^2\partial_{2t} + \cdots \\ \partial_\beta = \varepsilon\partial_{1\beta} \\ h_i = \varepsilon h_i^{(1)} + \varepsilon^2 h_i^{(2)} + \cdots \end{cases} \tag{A5}$$

where, $\varepsilon = \delta t$ and $D \equiv (\partial_t + e_{i\beta}\partial_\beta)$. In equation (A5), there is no "equilibrium" h_i term.

Retaining terms up to $O(\varepsilon^2)$ in equations (A4) and (A5) and substituting into equation (A3) results in equations in the consecutive order of the parameter ε:

$$O(\varepsilon^0) : \frac{\left(f_i^{(0)} - f_i^{\mathrm{eq}}\right)}{\tau} = 0 \tag{A6}$$

$$O(\varepsilon^1) : (\partial_{1t} + e_{i\beta}\partial_{1\beta}) f_i^{(0)} + \frac{f_i^{(1)}}{\tau - h_i^{(1)}} = 0 \tag{A7}$$

$$O(\varepsilon^2) : \partial_{2t} f_i^{(0)} + \left(1 - \frac{1}{2\tau}\right)(\partial_{1t} + e_{i\beta}\partial_{1\beta}) f_i^{(1)} + \frac{1}{2}(\partial_{1t} + e_{i\beta}\partial_{1\beta}) h_i^{(1)} + \frac{1}{\tau} f_i^{(2)} - h_i^{(2)} = 0 \tag{A8}$$

The distribution function f_i is constrained by equation (6) and the following equation (A9):

$$\sum_{i=0}^{8} f_i^{(m)} = 0, \quad \sum_{i=0}^{8} \mathbf{e}_i f_i^{(m)} = 0 \ \text{ for } \ m > 0 \tag{A9}$$

Note that $E^{(2n+1)} = 0$ for $n = 0,1,\ldots$ where E(n) are the tensors defined as $E^{(n)} = \sum_\alpha e_{\alpha 1} e_{\alpha 2} \ldots e_{\alpha n}$ and:

$$\sum_{i=1}^{4} e_{i\alpha} e_{i\beta} = 2\delta_{\alpha\beta} \tag{A10}$$

$$\sum_{i=5}^{8} e_{i\alpha} e_{i\beta} = 4\delta_{\alpha\beta} \tag{A11}$$

$$\sum_{i=1}^{4} e_{i\alpha}e_{i\beta}e_{i\gamma}e_{i\zeta} = 2\delta_{\alpha\beta\gamma\zeta} \tag{A12}$$

$$\sum_{i=5}^{8} e_{i\alpha}e_{i\beta}e_{i\gamma}e_{i\zeta} = 4\Delta_{\alpha\beta\gamma\zeta} - 8\delta_{\alpha\beta\gamma\zeta} \tag{A13}$$

where $\delta_{\alpha\beta}$ and $\delta_{\alpha\beta\gamma\zeta}$ are the Kronecker tensors, and:

$$\Delta_{\alpha\beta\gamma\zeta} = \delta_{\alpha\beta}\delta_{\gamma\zeta} + \delta_{\alpha\gamma}\delta_{\beta\zeta} + \delta_{\alpha\zeta}\delta_{\beta\gamma} \tag{A14}$$

With above properties of the tensor $\mathrm{E}^{(\mathrm{n})}$, we have:

$$\sum_{i=0}^{8} e_{i\alpha}e_{i\beta}f_i^{(0)} = \rho_0 u_\alpha u_\beta + p\delta_{\alpha\beta} \tag{A15}$$

$$\sum_{i=0}^{8} e_{i\alpha}e_{i\beta}e_{ik}f_i^{(0)} = \rho_0 c_s^2(\delta_{jk}\delta_{\beta\alpha} + \delta_{j\alpha}\delta_{\beta k} + \delta_{j\beta}\delta_{\alpha k})u_j \tag{A16}$$

Mass conservation and $\mathrm{h}_{\mathrm{i}}^{(1)}$
Summing on i in equation (A7), we obtain at $O(\varepsilon)$:

$$\partial_{1t}\rho + \partial_\beta \rho u_\beta = \sum_i h_i^{(1)} \tag{A17}$$

which motivates the following selection of $h_i^{(1)}$ when comparing with the target dynamics (of equations (A1) and (A2)). To recover the continuity equation (A1), because $\sum_i \omega_i = 1$, the following selection of $h_i^{(1)}$ is reasonable (Halliday *et al.*, 2001):

$$h_i^{(1)} = \frac{-\omega_i \rho u_r}{r} \tag{A18}$$

Then, we proceed to $O(\varepsilon^{2})$ now. Summing on i in equation (A8) gives:

$$\partial_{2t}\rho + \sum_i \frac{1}{2}\left(\partial_{1t} + e_{i\beta}\partial_{1\beta}\right)h_i^{(1)} - \sum_i h_i^{(2)} = 0 \tag{A19}$$

With our target dynamic in view, we obtain the equation (A20):

$$\sum_i \frac{1}{2}\left(\partial_{1t} + e_{i\beta}\partial_{1\beta}\right)h_i^{(1)} - \sum_i h_i^{(2)} = 0 \tag{A20}$$

equation (A20) can also be rewritten as equation (A21):

$$\sum_i h_i^{(2)} = \frac{1}{2}\sum_i (\partial_{1t} + e_{i\beta}\partial_{1\beta})h_i^{(1)} = \frac{1}{2}\left[\partial_{1t}\sum_i \frac{-\omega_i \rho u_r}{r}\right] = -\frac{1}{2}\left[\frac{\partial_{1t}\rho u_r}{r}\right] \tag{A21}$$

Momentum conservation and $h_i^{(2)}$

Multiplying equation (A7) with $e_{i\alpha}$ and summing over i, gives:

$$\partial_{1t}\rho u_\alpha + \partial_{1\beta}\Pi^0_{\alpha\beta} = \sum_i h_i^{(1)} e_{i\alpha} = 0 \tag{A22}$$

where, $\Pi^0_{\alpha\beta} = \sum_{i=1}^{8} e_{i\alpha}e_{i\beta}f_i^{(0)}$ is the zeroth-order of momentum flux tensor. With $\Pi^0_{\alpha\beta}$ given by equation (A15), using equation (A22) with $\alpha = r$, and substituting into (A21), we have a condition on $h_i^{(2)}$:

$$\sum h_i^{(2)} = \frac{1}{2r}\partial_\beta\left(c_s^2\rho\delta_{r\beta}\rho u_\beta u_r\right) \tag{A23}$$

The error in previous model of Halliday *et al.* (2001) partly lies in their opinion about equation (A22). It seems that Halliday *et al.* simply regarded terms $\partial_{1t}\rho u_\alpha + \partial_{1\beta}(\rho u_\alpha u_\beta)$ as the terms $D_t\rho u_\alpha = \partial_t\rho u_\alpha + \partial_\beta\rho u_\beta u_\alpha + \rho u_\alpha u_r/r$. Unfortunately, that is not true.

Multiplying equation (A8) with $e_{i\alpha}$ and summing over i gives:

$$\partial_{2t}\rho u_\alpha + \left(1 - \frac{1}{2\tau}\right)\partial_{1\beta}\Pi^{(1)}_{\alpha\beta} = -\frac{1}{2}\left(\partial_{1t}\sum_i e_{i\alpha}h_i^{(1)} + \partial_{1\beta}\sum_i e_{i\alpha}e_{i\beta}h_i^{(1)}\right) + \sum_i h_i^{(2)}e_{i\alpha} \tag{A24}$$

where, $\Pi^{(1)}_{\alpha\beta} = \sum e_{i\alpha}e_{i\beta}f_i^{(1)}$ is the first-order momentum flux tensor. With the aid of equations (A7) and (A16), we have:

$$\begin{aligned}
\Pi^{(1)}_{\alpha\beta} &= \sum_i e_{i\alpha}e_{i\beta}f_i^{(1)} = -\tau\sum_i e_{i\alpha}e_{i\beta}D_{1t}f_i^{(0)} + \tau\sum_i e_{i\alpha}e_{i\beta}h_i^{(1)} \\
&= -\tau\left[\sum_i \partial_{1t}\Pi^{(0)}_{\alpha\beta} + \partial_k\left(\sum_i e_{i\alpha}e_{i\beta}e_{ik}f_i^{(0)}\right)\right] + \tau\sum_i e_{i\alpha}e_{i\beta}h_i^{(1)} \\
&= -\tau\left[\sum_i \partial_{1t}\Pi^{(0)}_{\alpha\beta} + c_s^2(\delta_{\alpha\beta}\partial_j\rho u_j + \partial_\beta\rho u_\alpha + \partial_\alpha\rho u_\beta)\right] + \tau\sum_i e_{i\alpha}e_{i\beta}h_i^{(1)} \\
&\approx -\tau c_s^2\left[-\delta_{\alpha\beta}\rho\left(\partial_j u_j + \frac{u_r}{r}\right) + \rho(\delta_{\alpha\beta}\partial_j u_j + \partial_\beta u_\alpha + \partial_\alpha u_\beta)\right] - \tau c_s^2\delta_{\alpha\beta}\frac{\rho u_r}{r} + O(\varepsilon^2) \\
&= -\tau c_s^2\left[\rho(\partial_\beta u_\alpha + \partial_\alpha u_\beta)\right] + O(\varepsilon^2)
\end{aligned} \tag{A25}$$

Substituting equation (A25) into equation (A24) and using equations (A22) and (A24), we get:

$$\frac{\partial\rho u_\alpha}{\partial t} + \frac{\partial\rho u_\beta u_\alpha}{\partial x_\beta} + \frac{\partial p}{\partial x_\alpha} - \mu\frac{\partial^2 u_\alpha}{\partial x_\beta^2} - \mu\partial_\alpha(\nabla\cdot\mathbf{u}) = (1-\tau)c_s^2\partial_\alpha\left(\frac{\rho u_r}{r}\right) + \sum_i h_i^{(2)}e_{i\alpha} \tag{A26}$$

Compare momentum equation (A26) with equation (A2), to recover the NS momentum equations, equation (A27) should be satisfied:

$$(1-\tau)c_s^2\partial_\alpha\left(\frac{\rho u_r}{r}\right) + \sum_i h_i^{(2)}e_{i\alpha} = \frac{\rho\nu}{r}\left(\partial_r u_\alpha - \frac{1}{r}u_r\delta_{r\alpha}\right) - \frac{\rho u_\alpha u_r}{r} \tag{A27}$$

Solving equation system (A23) and (A27), we can obtain the expression of $h_i^{(2)}$:

$$h_i^{(2)} = \frac{\omega_i}{2r}\left[\partial_\beta\left(c_s^2\rho\delta_{r\beta} + \rho u_\beta u_r\right)\right] + 3\omega_i\left[\frac{\rho\nu}{r}\left(\partial_r u_\beta - \frac{1}{r}u_r\delta_{r\beta}\right)e_{i\beta} - \frac{\rho u_\beta u_r}{r}e_{i\beta}\right] - (1-\tau)\omega_i\partial_\beta\left(\frac{\rho u_r}{r}\right)e_{i\beta} \tag{A28}$$

The expression of $h_i^{(1)}$ (equation (A18)), $h_i^{(2)}$ (equation (A28)) are successfully derived and the continuity equation (A1) and NS equation (A2) can be fully recovered. In the model of Halliday *et al.* (2001), the mainly missing terms are relative to u_r. Although these terms may only slightly affect results of straight pipe flow, without these terms, the flows in constricted pipes cannot be simulated correctly.

Appendix 2

The stream-wise velocity profile (first-order slip-flow model) in a long microtube with rarefaction effect is given by Weng *et al.*(1999):

$$U(x,r) = -\frac{r_0^2}{4\mu}\frac{\partial p}{\partial x}\left[1 - \left(\frac{r}{r_0}\right)^2 + \frac{2\lambda}{r_0}\right] \tag{A29}$$

where λ is the molecular mean free path, r_O is the radius of the microtube. Since, $r_0 = D/2$ and local $Kn = \lambda/D$, using equations (21) and (A29), we have:

$$U(x,r) = -\frac{D^2}{16\mu}\frac{\mathrm{d}p}{\mathrm{d}x}\left(1 - 4\left(\frac{r}{D}\right)^2 + \frac{4Kn_\mathrm{o}}{\tilde{p}}\right) \tag{A30}$$

where $\tilde{p} = p(x,r)/p_\mathrm{o}$.

The pressure distribution in a long microtube is given by Weng *et al.* (1999) as:

$$S = -\frac{8}{\sqrt{\pi}} + \left\{\frac{64}{\pi} + S_\mathrm{in}^2 + \frac{16}{\sqrt{\pi}}S_\mathrm{in} + \left[\left(S_\mathrm{out}^2 - S_\mathrm{in}^2\right) + \frac{16}{\sqrt{\pi}}\left(S_\mathrm{out} - S_\mathrm{in}\right)\right]\tilde{x}\right\}^{\frac{1}{2}} \tag{A31}$$

where:

$$S = \left(Kn_\mathrm{o}\sqrt{\pi}\right)^{-1}\tilde{p}, S_\mathrm{in} = \left(Kn_\mathrm{o}\sqrt{\pi}\right)^{-1}Pr, S_\mathrm{out} = \left(Kn_\mathrm{o}\sqrt{\pi}\right)^{-1}, Pr = p_\mathrm{in}/p_\mathrm{o},$$

and $\tilde{x} = x/L$. L is the tube length. Hence, equation (A31) can also be rewritten as:

$$\tilde{p}(\tilde{x}) = -8Kn_\mathrm{o} + \sqrt{(8Kn_\mathrm{o})^2 + (1 + 16Kn_\mathrm{o})\tilde{x} + \left(Pr^2 + 16Kn_\mathrm{o}Pr\right)(1-\tilde{x})} \tag{A32}$$

From equation (A32) we can see that gas flowing in a long microtube with a significant pressure drop will also exhibit compressibility effects.

The mass-flow rate is computed by multiplying equation (A29) by the density and integrating across the tube. The dimensional mass-flow rate is given by Weng *et al.* (1999):

$$\dot{q} = -\frac{\pi\rho r_0^4}{2\mu}\frac{\partial p}{\partial x}\left[\frac{1}{4} + 2Kn\right] \tag{A33}$$

Hence, the dimensional mass flow rate at outlet of microtube is:

$$\dot{q} = -\frac{\pi\rho_\mathrm{o}D^4 p_\mathrm{o}}{16\mu L}\left(\frac{\partial\tilde{p}}{\partial\tilde{x}}\right)_\mathrm{o}\left[\frac{1}{8} + Kn_\mathrm{o}\right] \tag{A34}$$

The non-dimensional pressure gradient along the tube can be calculated from equation (A32) as:

$$\frac{\mathrm{d}\tilde{p}}{\mathrm{d}\tilde{x}} = \frac{1 - Pr^2 + 16Kn_{\mathrm{o}}(1 - Pr)}{2\sqrt{(8Kn_{\mathrm{o}})^2 + (1 + 16Kn_{\mathrm{o}})\tilde{x} + \left(Pr^2 + 16Kn_{\mathrm{o}}Pr\right)(1 - \tilde{x})}} \tag{A35}$$

Hence, equation (A34) can also be written as:

$$\dot{q} = \frac{\pi D^4 p_o^2}{256\mu \mathrm{LRT}} \left[(Pr^2 - 1) + 16Kn_{\mathrm{o}}(Pr - 1)\right] \tag{A36}$$

In addition, the mass-flow rate for the continuum gas (without the rarefaction effect) is:

$$(\dot{q})_{\mathrm{continuum}} = -\frac{\pi D^4}{256\mu \mathrm{RT}} \frac{\partial(p^2)}{\partial x} = \frac{\pi D^4 p_o^2}{256\mu \mathrm{RT}} \frac{(Pr^2 - 1)}{L} \tag{A37}$$

Corresponding author
Haibo Huang can be contacted at: g0301108@nus.edu.sg